CORE
Metadata, citation and similar papers at core.ac.uk
Provided by Nottingham ePrints

The University of Nottingham
UNITED KINGDOM · CHINA · MALAYSIA

Evans, J.D. and King, J.R. (2017) Stress-dependent local oxidation of silicon. SIAM Journal on Applied Mathematics, 77 (6). pp. 2012-2039. ISSN 0036-1399

**Access from the University of Nottingham repository:**
http://eprints.nottingham.ac.uk/50646/1/evans%20and%20king%20-%20stress%20dependent%20local%20oxidation%20of%20silicon.pdf

**Copyright and reuse:**

The Nottingham ePrints service makes this work by researchers of the University of Nottingham available open access under the following conditions.

This article is made available under the University of Nottingham End User licence and may be reused according to the conditions of the licence. For more details see: http://eprints.nottingham.ac.uk/end_user_agreement.pdf

**A note on versions:**

The version presented here may differ from the published version or from the version of record. If you wish to cite this item you are advised to consult the publisher's version. Please see the repository url above for details on accessing the published version and note that access may require a subscription.

For more information, please contact eprints@nottingham.ac.uk

# Stress dependent local oxidation of silicon

J.D. Evans * and J.R. King †

October 19, 2017

**Abstract**

The two-dimensional isolation oxidation of silicon is considered for stress dependent reaction and diffusion coefficients. The influence of such parameters is investigated numerically and asymptotically in the bird's beak problem and for curved geometries arising in the oxidation of cylindrical and spherical structures. In the bird's beak problem, the limit of large activation volume is described for a stress dependent reaction coefficient, illustrating the significant growth retardation of the silicon/silicon oxide interface and reduced stresses in the silicon oxide. Novel high order nonlinear evolution type PDEs are derived and investigated using asymptotic and numerical techniques.

*Keywords: silicon oxidation; stress dependent reaction coefficient; matched asymptotic expansions.*

*AMS Classification: 75R50, 76D07, 35C20.*

## 1 Introduction

The local oxidation of silicon (LOCOS) is a well-studied process (first reported by Appels et al. [4]) in which oxide is selectively grown on part of a silicon wafer during the fabrication of an integrated circuit. This selective oxidation is achieved by masking the parts of the silicon surface where devices will be formed with silicon nitride. Growth of oxide (known as the field oxide) then occurs by the thermal oxidation of the unmasked silicon, the nitride being impervious to oxidant. Before the deposition of the nitride mask, a thin oxide (known as the pad oxide) is grown on the silicon in order to reduce the stresses that result from, in particular, the different thermal expansion coefficients of the silicon and the nitride. Since oxidant is able to diffuse laterally under the mask through the pad oxide, the resulting oxide has a characteristic shape known as a 'bird's beak'. An alternative isolation technique to LOCOS is trench isolation, particularly for sub-0.5$\mu$m devices. Here a trench is etched into the silicon substrate and subsequently oxidised and then filled with oxide [36, 6].

However, stress effects in silicon oxidation have been suspected since Marcus and Sheng [25] observed oxidation rate retardation around convex and concave corners of silicon trenches. These effects were clarified through experiment by Kao et al. [16, 17] in which the oxidation of concave and convex cylindrical structures were measured. The quantified stress effects were incorporated into the oxidation model through stress-dependent parameters, the key ones being the silicon/oxide surface reaction rate $\bar{k}_s$, the oxidant diffusivity in the oxide $\bar{D}_s$, the equilibrium oxidant concentration $\bar{c}_s^*$ and the oxide viscosity $\bar{\mu}_s$. These were originally suggested by Kao et al. [17] for the cylindrical geometries and subsequently used by other authors (for example, [34, 39, 40]) in modelling LOCOS and trench oxidation. Recent applications include the oxidation of silicon nanostructures, such as Si nanowires (SiNW), Si nanocrystals and Si nanotrenches [7, 33, 28, 19]. Stress effects and understanding retarded oxidation rates are now even more pressing as dimensions are substantially smaller [1, 12, 13, 23, 14, 15].

In this work, we propose to investigate the effect of stress-dependent parameters on the higher-dimensional generalisation of the classical Deal-Grove model for silicon oxidation [9] in both cylindrical structures and the LOCOS process. Attention will be focused upon the effect of the stress-dependent reaction coefficient, which will be taken to depend upon the normal stress acting on the $Si/SiO_2$ interface. This dependence is taken in the form

$$\bar{k}_s = \begin{cases} \bar{k}_0 \exp\left(\frac{V_k}{kT}\bar{\sigma}_{nn}\right), & \text{if } \bar{\sigma}_{nn} \leq 0, \\ \bar{k}_0, & \text{if } \bar{\sigma}_{nn} > 0, \end{cases} \tag{1.1}$$

in accordance with [40, 34, 32]. Here, $\bar{k}_0$ is the stress free value of $\bar{k}_s$, $k$ is Boltzman's constant, $T$ is temperature, $V_k$ being the so-called 'reaction jump or activation volume' and $\bar{\sigma}_{nn}$ is the normal stress exerted on the oxide by the silicon at the silicon/oxide interface. In the original work of [17], $V_k = 25\mathring{A}^3$ is taken as the difference between the molecular volume of $SiO_2$ and atomic volume of Si, so that the product $V_k\sigma_{nn}$ gives the additional work carried out by the expanding new oxide and is added to the activation energy. In [34], half the value $V_k = 12.5\mathring{A}^3$ is taken, the authors arguing that only one bridging oxygen atom is placed between each broken Si-Si bond.

*Department of Mathematical Sciences, University of Bath, Bath, BA2 7AY. U.K.
†School of Mathematical Sciences, University of Nottingham, University Park, Nottingham, NG7 2RD. U.K.

Kao et al. [17] also refer to early work on high-pressure effects (see [5] and [27]) to suggest that the oxidant diffusivity and equilibrium concentration (i.e. oxidant solubility) are decreased under high pressure. The proposed empirical forms are

$$\bar{D}_s = \begin{cases} D_0 \exp\left(-\frac{V_d}{kT}\bar{p}\right), & \text{if } \bar{p} \geq 0, \\ D_0, & \text{if } \bar{p} < 0, \end{cases} \quad \bar{c}_s^* = \begin{cases} c_0^* \exp\left(-\frac{V_c}{kT}\bar{p}\right), & \text{if } \bar{p} \geq 0, \\ c_0^*, & \text{if } \bar{p} < 0, \end{cases} \tag{1.2}$$

where $D_0$ and $c_0^*$ are the stress free values, $\bar{p}$ denotes the pressure in the oxide, $V_d$ and $V_c$ are the diffusion and solubility activation volumes. The temperature dependence of the solubility coefficient is questionnable (see [9]) and has a weaker dependence on the oxide stress than either the reaction or diffusion coefficients. It is argued in [34] that it should be treated as constant. It is worth remarking that all the activation volumes $V_k, V_d, V_c$ are usually treated as fitting parameters by various authors and determined from experimental data of the oxidation of concave and convex silicon structures e.g. [39, 34]. The diffusion activation volume $V_d$ is particularly difficult to obtain a consistent temperature-independent value from experimental data. For this reason it was discarded in the original work of [17], whilst in [34] a cut off value is introduced for it. The numerical simulations of [39] suggest it may influence the oxidation of concave corners, but not convex corners. A first-principles study for the variation of the $O_2$ diffusion coefficient at a microscopic level and its retardation under pressure is given in [2], which supports the use of the form above in (1.2). A similar investigation for the reaction coefficient is given in [3]. As such, it seems that the principle of macroscopic work appears plausible in applicability to the reaction on an atomic scale.

In regard to the oxide viscosity, [17], Seidl et al. [30] and [39] assume a simple exponential pressure dependence,

$$\bar{\mu}_s = \begin{cases} \mu_0 \exp(\bar{\alpha}_v \bar{p}), & \text{if } \bar{p} \leq 0, \\ \mu_0, & \text{if } \bar{p} > 0, \end{cases} \tag{1.3}$$

where $\mu_0$ is the stress free value and $\bar{\alpha}_v$ is an empirical parameter. Typical values for these parameters over a range of temperatures are given in [17]. In [34], it is argued that the shear-stress is a more important factor than pressure in determining the oxide's viscosity. Consequently the authors adopt a functional form for shear-stress-dependent oxide viscosity based on Eyring's nonlinear flow model (see also [32]). However, as remarked by King [20], an analysis of the relevant models shows that the behaviour typically depends much more strongly on the oxidant transport model than on the flow model. Furthermore, since little empirical evidence is available to guide the choice of constitutive relation for the oxide (although [37, 38] and [32] have tried to address this issue), the added complexity introduced by a stress-dependent viscosity is unnecessary at this stage. This is further supported by [39], who found that the viscosity form (1.3) had little effect on the altering oxide thickness at corners.

In summary, our main focus will be on the stress-dependent reaction and diffusion coefficients, there being more certainty in regards to their modelling and physical basis for stress variation. Although we retain a pressure dependent diffusion coefficient, we only quantify its effects in cylindrical geometries, where it is known to play a role. The other parameters of solubility and viscosity will be treated as constant. It is worth explicitly stating that the elastic deformation time-scale during new oxide creation is far shorter than the subsequent viscous flow deformation and oxidant diffusion. This is due to the fast nature of the oxide reaction and thus we neglect such elastic effects. Treatment of the oxide as viscoelastic (or even elastic at lower temperatures) requires specifying the stress for new oxide formation and will thus include the neglected elastic effects. However, these more complicated constitutive models will be pursued elsewhere.

The model equations for the two-dimensional LOCOS problem are discussed in detail in [21, 22] and form a moving boundary problem. Important goals of the modelling are to determine conditions that minimize both the lateral extent of oxidation (the length of the bird's beak) and the oxidation-induced stresses. Here then, we shall consider the effect of a stress-dependent reaction coefficient on the development of the moving boundaries. The model takes the oxidant diffusion to be quasi-steady, since the diffusion time-scale is far smaller than that associated with the movement of the $Si/SiO_2$ interface from the reaction. The oxide is treated as a highly viscous incompressible Newtonian fluid, satisfying the slow flow equations with inertia neglected. The nitride mask is treated as a light plate or elastica, with bending rigidity but negligible mass and silicon is treated as rigid and impervious to the oxidant. The relevant geometry is illustrated in Fig. 1. A key aspect of the process is that the oxide occupies $\gamma \approx 2.27$ times the volume of silicon from which it was formed. It is this volume expansion which drives the flow of the oxide. Following [21] and modifying for stress-dependent parameters, the resulting non-dimensional model for the oxidant concentration $c(x, y, t)$ is

$$\frac{\partial}{\partial x}\left(D_s \frac{\partial c}{\partial x}\right) + \frac{\partial}{\partial y}\left(D_s \frac{\partial c}{\partial y}\right) = 0,$$

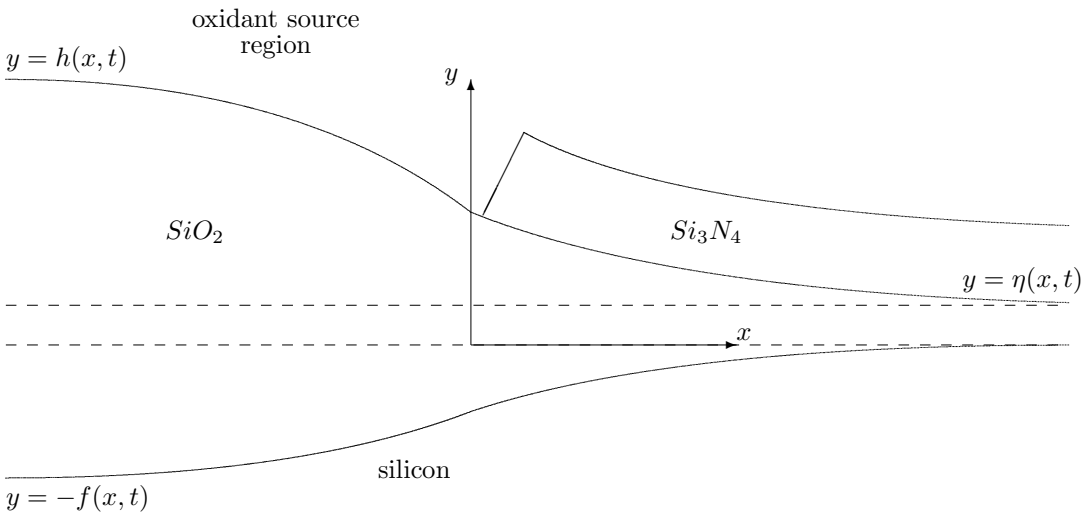


Figure 1: Schematic illustration of the bird's beak geometry. The dashed lines indicate the edges of the initial pad oxide.

$$
\begin{aligned}
&\text{on } \ y = -f && D_s \frac{\partial c}{\partial n} = -k_s\, c, \qquad \gamma \frac{\partial f}{\partial t} = D_s \left( \frac{\partial c}{\partial y} + \frac{\partial f}{\partial x}\frac{\partial c}{\partial x} \right), \\
&\text{on } \ y = h && D_s \frac{\partial c}{\partial n} = H(1-c), \\
&\text{on } \ y = \eta && \frac{\partial c}{\partial n} = 0, \\
&\text{as } \ x \to -\infty && \frac{\partial c}{\partial x} \to 0, \\
&\text{as } \ x \to +\infty && c \to 0, \ \ f \to 0, \ \ \eta \to 1, \\
&\text{at } \ t = 0 && f = 0, \ \ \eta = 1, \ \ h = 1,
\end{aligned} \tag{1.4}
$$

whilst that for the flow problem is

$$
\mu_s \left( \frac{\partial^2 \psi}{\partial y^2} - \frac{\partial^2 \psi}{\partial x^2} \right) = -\frac{\partial^2 A}{\partial x \partial y}, \qquad \frac{\partial^2 A}{\partial y^2} - \frac{\partial^2 A}{\partial x^2} = 4\mu_s \frac{\partial^2 \psi}{\partial x \partial y}, \qquad p = -\frac{1}{2}\nabla^2 A,
$$

$$
\begin{aligned}
&\text{on } \ y = -f && \frac{\partial \psi}{\partial n} = 0, \qquad \frac{\partial \psi}{\partial s} = (\gamma - 1)\frac{\partial f}{\partial t}\left( 1 + \left( \frac{\partial f}{\partial x} \right)^2 \right)^{-1/2}, \\
&\text{on } \ y = \eta && \frac{\partial \psi}{\partial n} = 0, \qquad A = -F^* \frac{\partial^2 \eta}{\partial x^2}\left( 1 + \left( \frac{\partial \eta}{\partial x} \right)^2 \right)^{-3/2}, \qquad \frac{\partial \eta}{\partial t} = -\left( \frac{\partial \psi}{\partial x} + \frac{\partial \eta}{\partial x}\frac{\partial \psi}{\partial y} \right), \\
&\text{on } \ y = h && A = \frac{\partial A}{\partial n} = 0, \qquad \frac{\partial h}{\partial t} = -\left( \frac{\partial \psi}{\partial x} + \frac{\partial h}{\partial x}\frac{\partial \psi}{\partial y} \right), \\
&\text{as } \ x \to -\infty && A \to 0, \ \ \frac{\partial \psi}{\partial y} \to 0, \\
&\text{as } \ x \to +\infty && A \to \beta(t)(y-1), \ \ \psi \to 0.
\end{aligned} \tag{1.5}
$$

All lengths have been made dimensionless with the initial pad oxide thickness $a$. Here, $\psi$ and $A$ are the stream function and Airy stress function of the oxide, with the latter being a convenient representation for the inertialess momentum equation. The coupled relationships in (1.5) follow from the constitutive equation of a Newtonian viscous fluid and retained in this form for a dimensionless viscosity function $\mu_s$. In the constant viscosity case $\mu_s = 1$, decoupling the equations gives rise to the biharmonic equation for both variables. In (1.4) and (1.5), $y = -f(x,t)$ is the oxide/silicon interface, $y = h(x,t)$ is the oxide/gas interface and $y = \eta(x,t)$ is the oxide/nitride interface. All three interfaces must be determined as part of the solution as does the far-field function $\beta(t)$ in the Airy stress function. The constants $H$ and $F^*$ are the non-dimensional gas phase transport

| T $^0$C | | $\bar{k}_0$ (cm/s) | $D_0$ (cm$^2$/s) | $c_0^*$ (cm$^{-3}$) | $\mu_0$ (poise) | $\mu_0 D_0/\lambda a^2$ (Pa) | $k_0$ | $\alpha_k$ |
|---|---|---|---|---|---|---|---|---|
| 800 | (dry) | $3.61 \times 10^{-5}$ | $9.00 \times 10^{-10}$ | $5.2 \times 10^{16}$ | $1.0 \times 10^{15}$ | $8.51 \times 10^{11}$ | $2.01 \times 10^{-4}$ | 14 |
| | (wet) | $1.89 \times 10^{-6}$ | $1.87 \times 10^{-10}$ | $3.0 \times 10^{19}$ | $1.0 \times 10^{15}$ | $5.09 \times 10^{13}$ | $5.05 \times 10^{-5}$ | 859 |
| 900 | (dry) | $2.07 \times 10^{-4}$ | $2.65 \times 10^{-9}$ | $5.2 \times 10^{16}$ | $3.0 \times 10^{14}$ | $7.52 \times 10^{11}$ | $3.91 \times 10^{-4}$ | 11 |
| | (wet) | $1.16 \times 10^{-5}$ | $3.89 \times 10^{-10}$ | $3.0 \times 10^{19}$ | $3.0 \times 10^{14}$ | $3.18 \times 10^{13}$ | $1.49 \times 10^{-4}$ | 490 |
| 1000 | (dry) | $8.53 \times 10^{-4}$ | $6.58 \times 10^{-9}$ | $5.2 \times 10^{16}$ | $3.0 \times 10^{13}$ | $1.87 \times 10^{10}$ | $6.48 \times 10^{-4}$ | 2.7 |
| | (wet) | $5.30 \times 10^{-5}$ | $7.21 \times 10^{-10}$ | $3.0 \times 10^{19}$ | $3.0 \times 10^{13}$ | $5.89 \times 10^{12}$ | $3.68 \times 10^{-4}$ | 84 |
| 1100 | (dry) | $3.61 \times 10^{-3}$ | $1.43 \times 10^{-8}$ | $5.2 \times 10^{16}$ | $6.0 \times 10^{12}$ | $8.11 \times 10^{10}$ | $1.26 \times 10^{-3}$ | 1 |
| | (wet) | $1.94 \times 10^{-4}$ | $1.22 \times 10^{-9}$ | $3.0 \times 10^{19}$ | $6.0 \times 10^{12}$ | $1.99 \times 10^{12}$ | $7.99 \times 10^{-4}$ | 26 |
| 1200 | (dry) | $1.32 \times 10^{-2}$ | $3.53 \times 10^{-8}$ | $5.2 \times 10^{16}$ | $6.0 \times 10^{11}$ | $2.00 \times 10^{10}$ | $1.87 \times 10^{-3}$ | 2.5 |
| | (wet) | $5.87 \times 10^{-4}$ | $2.29 \times 10^{-9}$ | $3.0 \times 10^{19}$ | $6.0 \times 10^{11}$ | $3.74 \times 10^{11}$ | $1.28 \times 10^{-3}$ | 46 |

Table 1: Selected parameter values for dry and wet oxidation over a range of processing temperatures taken from [17, 42]. Calculated are the stress scaling as well as the non-dimensional stress-free reaction coefficient and activation volume. A representative pad-oxide thickness of $a = 50$Å has been used together with $\lambda$ as given in the text.

coefficient and nitride rigidity. The non-dimensional stress dependent reaction and diffusion coefficients $k_s, D_s$ take the form,

$$k_s = \begin{cases} k_0 \exp\left(\alpha_k \sigma_{nn}\right), & \text{if } \sigma_{nn} \leq 0, \\ k_0, & \text{if } \sigma_{nn} > 0, \end{cases} \qquad D_s = \begin{cases} \exp(-\alpha_d p), & \text{if } p \geq 0, \\ 1, & \text{if } p < 0, \end{cases} \tag{1.6}$$

where $k_0$ is the dimensionless stress free reaction coefficient and the dimensionless activation parameters $\alpha_k, \alpha_d$ are defined as

$$k_0 = \frac{a\bar{k}_0}{D_0}, \qquad \alpha_k = \frac{V_k \mu_0 D_0}{kT\lambda a^2}, \qquad \alpha_d = \frac{V_d}{V_k}\alpha_k. \tag{1.7}$$

Here $\mu_0 D_0/\lambda a^2$ is the characteristic stress scaling with $a$ denoting the initial pad oxide thickness, $\lambda = N/c_0^*\gamma$ and $N$ being the number of oxidant molecules which react with a unit volume of silicon. Oxidation may take place using oxygen (dry) or steam (wet), the chemical reaction being different for each oxidant (see [35]). We have

$$N = \begin{cases} 5 \times 10^{22} & \text{(dry)}, \\ 10 \times 10^{22} & \text{(wet)}, \end{cases} \qquad \lambda = \begin{cases} 4.23 \times 10^5 & \text{(dry)}, \\ 1.47 \times 10^3 & \text{(wet)}, \end{cases}$$

using values for $N$ from [35] and the equilibrium concentration $c_0^*$ in Table 1 to determine the ratio $\lambda$. Table 1 then gives estimates of the characteristic stress scaling as well as the dimensionless stress free reaction coefficient $k_0$ and dimensionless reaction activation volume $\alpha_k$. Consequently we have the parameter ranges

$$10^{-3} \leq k_0 \leq 10^{-6}, \qquad 1 \leq \alpha_k \leq 10^3, \tag{1.8}$$

suggesting that we are in the asymptotic regime of the reaction-controlled case ($k_0 \ll 1$) with potentially large activation volume $\alpha_k \geq O(1)$.The ratio $V_d/V_k$ can vary between 4 and 8 (when extracted from experimental data fitting [31]), suggesting that the diffusion coefficient is more sensitive to the oxide stress than is the reaction coefficient. The normal stress $\sigma_{nn}$ has the following expression,

$$\sigma_{nn} = -p + 2\mu_s(\gamma - 1)\frac{\partial f}{\partial t}\frac{\partial^2 f}{\partial x^2}\left(1 + \left(\frac{\partial f}{\partial x}\right)^2\right)^{-3/2}, \tag{1.9}$$

which is derived in Appendix A. In a similar manner, we may calculate the components of the total force exerted by the oxide on the nitride interface $y = \eta(x,t)$. From [21], we have that

$$\int_0^{+\infty} \sigma_{nx} ds = -\left[\frac{\partial A}{\partial y}\right]_0^{+\infty} = -\beta(t), \qquad \int_0^{+\infty} \sigma_{ny} ds = \left[\frac{\partial A}{\partial x}\right]_0^{+\infty} = 0, \tag{1.10}$$

where is $s$ is the distance along the interface and $n$ the outward normal from the oxide. As such we may interpret $\beta$ as representing the the total force exerted by the oxide on the nitride in the x-direction, whilst we note that the total vertical force on the nitride is zero.

The layout of the paper is as follows. In Section 2 we consider the two-dimensional case of the bird's beak problem in the reaction-controlled limit. Using slowly-varying behaviour (due to the small aspect ratio geometry under the nitride mask), a coupled system of PDEs is derived to describe the pressure in the oxide and growth of the interfaces. The system is investigated numerically and in the asymptotic limit of large activation volume. In Section 3, we discuss the oxidation of curved surfaces for cylindrical and spherical geometries, which aids understanding and comparison of the effect of stress dependent parameters to experimental work. The viscosity will be treated as constant $\mu_s = 1$ from now on, although our derivation of (1.9) and the form of the oxide's slow flow equations, show that a varying viscosity function can easily be included.

## 2 The bird's beak problem: reaction-controlled case

In this section, we discuss the case of reaction-controlled oxidation, concerning ourselves with the behaviour of the oxide beneath the nitride mask. We state the leading order problem describing the slowly-varying behaviour under the mask for the most complicated coupling between the concentration and flow problems. The method of derivation closely follows the stress independent case discussed in [22], so much of the detail is omitted. The stress-independent case is given by taking $\alpha_k = 0$ in the analysis below.

The limit $k_0 \to 0$, corresponds to the reaction controlled case in which the oxidation reaction at the $Si/SiO_2$ interface is the rate-limiting step. We introduce the scalings

$$k_0 = \epsilon^2 \kappa_0, \qquad \tau = \epsilon^2 t, \tag{2.1}$$

where $\epsilon \ll 1$ and $\kappa_0 = O(1)$. Table 1 gives estimates of $\epsilon$ from $10^{-1}$ to $10^{-3}$ and which will be even smaller for thinner pad oxides. Two regions need to be considered, namely that near the mask edge in which $x = O(1)$ and a slowly-varying region far under the mask where $x = O(\epsilon^{-1})$. In the mask edge region, stresses and flow are smaller than under the mask (see [22]) i.e. $p = O(\epsilon)$ and consequently we may use the one-dimensional stress-independent solution for the oxidant concentration and growth of the $Si/SiO_2$ interface, namely

$$c \sim 1, \qquad f \sim \frac{\kappa_0}{\gamma}\tau, \tag{2.2}$$

We are thus within the linear growth regime of the Deal-Grove solution [9]. The oxidation process ceases to be reaction controlled when $\tau = O(\epsilon^{-2})$, when the quadratic correction terms for the $Si/SiO_2$ interface growth are no longer small compared to the leading order linear growth term. Although the nitride is assumed inextensible, the edge of the nitride during its bending may be taken at $x = 0$ since its variation is $O(\epsilon)$ and thus small (see [21]).

Under the mask, we introduce the slowly varying $x$ variable

$$X = \epsilon x,$$

where $X > 0$ and now consider the region $X = O(1)$. In the limit $\epsilon \to 0$, the concentration problem leads to the expansions

$$f \sim f_0(X,\tau), \qquad \eta \sim \eta_0(X,\tau), \qquad c \sim \frac{\gamma}{\kappa_{s0}}\frac{\partial f_0}{\partial \tau}, \qquad p \sim p_0(X,\tau),$$

in $X = O(1)$, $X > 0$, where $f_0$ is governed by

$$\frac{\partial f_0}{\partial \tau} = \frac{\partial}{\partial X}\left((\eta_0 + f_0)D_{s0}(p_0)\frac{\partial}{\partial X}\left(\frac{1}{\kappa_{s0}(p_0)}\frac{\partial f_0}{\partial \tau}\right)\right), \tag{2.3}$$

with

$$\kappa_{s0}(p_0) = \begin{cases} \kappa_0 e^{-\alpha_k p_0}, & \text{if } p_0 > 0, \\ \kappa_0, & \text{if } p_0 \le 0, \end{cases} \qquad D_{s0} = \begin{cases} e^{-\alpha_d p_0}, & \text{if } p_0 > 0, \\ 1, & \text{if } p_0 \le 0. \end{cases} \tag{2.4}$$

Here $p_0(X,\tau)$ is the leading-order pressure in the oxide, which is given below in (2.8). Since (2.2) hold in $x = O(1)$ i.e. $X = O(\epsilon)$, we have the following boundary condition from matching at the mask edge,

$$\text{at } X = 0 \qquad f_0 = \frac{\kappa_0}{\gamma}\tau, \tag{2.5}$$

together with the far-field condition

$$\text{as } X \to +\infty \qquad f_0 \to 0 \tag{2.6}$$

and the initial condition

$$\text{at } \tau = 0 \qquad f_0 = 0. \tag{2.7}$$

This then brings us to the flow problem which depends on the rigidity of the nitride. The most complicated balance (i.e. the distinguished limit) is given by

$$F^* = R\epsilon^{-4},$$

where $R = O(1)$. The normal stresses are $O(1)$ within the oxide and thus have a significant effect on the reaction and diffusion coefficients. We have at leading order

$$\sigma_{11} = \frac{\partial^2 A}{\partial x^2}, \sigma_{22} = \frac{\partial^2 A}{\partial y^2} \sim -R\frac{\partial^4 \eta_0}{\partial X^4}, \quad \sigma_{12} = -\frac{\partial^2 A}{\partial x \partial y} \sim \epsilon R\frac{\partial^5 \eta_0}{\partial X^5}\left(y - \frac{1}{2}(\eta_0 - f_0)\right), \quad p \sim p_0 = R\frac{\partial^4 \eta_0}{\partial X^4}, \tag{2.8}$$

on using similar expansions to those in section 2.2 of [22], which give the normal and shear stresses, as well as the pressure. The leading order equations for the motion of the interfaces are then completed by the lubrication equation

$$\frac{\partial \eta_0}{\partial \tau} - (\gamma - 1)\frac{\partial f_0}{\partial \tau} = \frac{R}{12}\frac{\partial}{\partial X}\left((\eta_0 + f_0)^3 \frac{\partial^5 \eta_0}{\partial X^5}\right), \tag{2.9}$$

together with the boundary conditions (after matching into $x = O(1)$),

$$\text{at } X = 0 \qquad \frac{\partial^2 \eta_0}{\partial X^2} = \frac{\partial^3 \eta_0}{\partial X^3} = \frac{\partial^4 \eta_0}{\partial X^4} = 0, \tag{2.10}$$

$$\text{as } X \to +\infty \qquad \eta_0 \to 1, \tag{2.11}$$

$$\text{at } \tau = 0 \qquad \eta_0 = 1. \tag{2.12}$$

We remark that the third condition in (2.10) when used in (2.8), is consistent with the pressure being small in the mask edge region. The expression for the leading order pressure is as expected from Euler-Bernoulli beam theory for an elastica and its independence of depth consistent with lubrication theory.

The complete system is now given by (2.3)–(2.7) together with (2.9)–(2.12). We remark that the pressure $p = O(1)$ in $X = O(1)$ and is substantially smaller $p = O(\epsilon)$ in the mask edge region $X = O(\epsilon)$ (as stated earlier). Thus stress-independent growth is appropriate for the mask edge condition in (2.5) if $\alpha_k = o(1/\epsilon)$. However, if $\alpha_k = O(1/\epsilon)$, then stress-dependent growth becomes appropriate at the mask edge and the matching conditions (2.5) and (2.10) require modification. Table 1 suggests that both activation volume regimes are appropriate. We consider first, numerical solution of the system appropriate to $\alpha_k = o(1/\epsilon)$, before addressing the large activation volume asymptotics relevant to $\alpha_k = O(1/\epsilon)$ case.

## 2.1 Numerical results

Numerical solution of the system (2.3)–(2.7), (2.9)–(2.12) was obtained using COMSOL Multiphysics. The system can be written in terms of second-order equations using the dependent variables $u_1 = f_0, u_2 = \eta_0, u_3 = \gamma f_{0\tau}/\kappa_{s0}, u_4 = \eta_{0XX}, u_5 = p_0$, so that the governing equations take the form

$$\frac{\partial u_1}{\partial \tau} - \frac{\kappa_{s0}}{\gamma} u_3 = 0, \qquad \frac{\partial u_2}{\partial \tau} - \left(\frac{\gamma - 1}{\gamma}\right) \kappa_{s0} u_3 - \frac{\partial}{\partial X}\left(\frac{(u_1 + u_2)^3}{12} \frac{\partial u_5}{\partial X}\right) = 0,$$

$$-\frac{\partial}{\partial X}\left((u_1 + u_2) D_{s0} \frac{\partial u_3}{\partial X}\right) + \kappa_{s0} u_3 = 0, \quad -\frac{\partial^2 u_2}{\partial X^2} + u_4 = 0, \quad -R \frac{\partial^2 u_4}{\partial X^2} + u_5 = 0.$$

These were then implemented in the PDE, Coefficient Form Application Mode using the Time-Dependent Analysis solver. The numerical spatial domain was taken as $[0, 50]$ with 7680 equal length quadratic Lagrange elements. Solver tolerances were set at Abs= $10^{-3}$, Rel= $10^{-2}$ with default BDF time-stepping and linear system solver Direct (UMFPACK). Figures 2 and 3 illustrate the effect of the stress-dependent reaction coefficient on the oxide interfaces $-f_0, \eta_0$ and the pressure $p_0$ under the nitride mask. Model parameters used are given in the figure legend. The stress-dependent reaction coefficient does not appear to have a discernable affect on the pressure nor the interfaces until the larger values of the stress dependent parameter $\alpha_k$ in Figure 3. The oscillatory nature of the pressure is a consequence of the total vertical force on the nitride needing to be zero from (1.10), and thus the stress-dependent reaction coefficient does not deviate uniformly from its stress-free value with lateral distance under the mask. Added to which, the relatively small numerical values of the pressure indicates that large values of $\alpha_k$ are required before significant stress effects are noticeable. The pressure profiles shown here, are qualitatively similar to the normal stress plots in [8] using full 2D LOCOS simulation software. Large compressive stress peak is found near to the nitride mask edge and a large tensile peak further under it.

## 2.2 Large activation volume asymptotics

We consider here the large $\alpha_k$ limit, corresponding to large activation volume for the reaction coefficient. Further, we'll address the the distinguished limit $\alpha_k = O(1/\epsilon)$, in which stress-dependent growth now occurs at the mask edge as well as under far under the mask. Since $p = O(\epsilon)$ (we'll take $p = \epsilon P_0$ for definiteness) in the mask edge region $X = O(\epsilon)$, the matching conditions (2.5) and (2.12) for the $X = O(1)$ problem require modification to

$$\text{at } X = 0 \qquad f_0 = \frac{\hat{\kappa}_{s0}(P_0)}{\gamma}\tau, \qquad \frac{\partial^2 \eta_0}{\partial X^2} = \frac{\partial^3 \eta_0}{\partial X^3} = 0, \ \frac{\partial^4 \eta_0}{\partial X^4} = \frac{P_0}{R\,\alpha_k} \tag{2.13}$$

where

$$\hat{\kappa}_{s0}(P_0) = \begin{cases} \kappa_0 e^{-P_0}, & \text{if } P_0 > 0, \\ \kappa_0, & \text{if } P_0 \le 0. \end{cases} \tag{2.14}$$

Here $P_0$ is prescribed e.g. from the one-dimensional solution of the field-oxide growth and although can be time-varying, we will take it to be constant. The fourth condition in (2.13) is the pressure matching condition $p_0 \sim P_0/\alpha_k$ as $X \to 0$.

The large $\alpha_k$ limit gives a three-region structure, where we will need to consider an outer region $X = O(\alpha_k^{\frac{1}{4}})$ in which a moving front $X = S(\tau)$ arises where the Si/SiO$_2$ interface vanishes, an inner region of width $\alpha_k^{-\frac{1}{4}}$

FIG1S.pdf

Figure 2: Effect of a stress-dependent reaction coefficient for moderate $\alpha_k$. Plotted are the interfaces $-f_0, \eta_0$ and the pressure $p_0$ at selected times for the three values $\alpha_k = 0, 1, 10$. The other model parameter values being $R = 1, \kappa_0 = 1, \gamma = 2.27, D_{s0} = 1$.

FIG2Sb.pdf

Figure 3: Effect of a stress-dependent reaction coefficient for large values of $\alpha_k$. Plotted are the interfaces $-f_0, \eta_0$, the pressure $p_0$ at selected times for large values $\alpha_k = 100$ and 1000. The other model parameter values being $R = 1, \kappa_0 = 1, \gamma = 2.27, D_{s0} = 1$.

about the moving front and finally a region ahead of this front where the Si/$SiO_2$ interface is exponentially small. For convenience, we introduce the the variable

$$u = \frac{\partial^2 \eta_0}{\partial X^2}, \tag{2.15}$$

where $p_0 = R u_{XX}$. We first introduce the scalings

$$X = \alpha_k^{\frac{1}{4}} \hat{X}, \qquad \tau = \alpha_k^{\frac{1}{2}} \hat{\tau}, \qquad f_0 = \alpha_k^{\frac{1}{2}} \hat{f}, \qquad \eta_0 = \hat{\eta}, \qquad u = \frac{\hat{u}}{\alpha_k^{\frac{1}{2}}}, \qquad p_0 = \frac{1}{\alpha_k} \hat{p}, \tag{2.16}$$

into the system (2.3)–(2.7), (2.9)–(2.12) with modification (2.13) to obtain

$$\frac{\partial \hat{f}}{\partial \hat{\tau}} = \frac{\partial}{\partial \hat{X}} \left( \left( \frac{\hat{\eta}}{\alpha_k^{\frac{1}{2}}} + \hat{f} \right) \frac{\partial}{\partial \hat{X}} \left( \frac{1}{\kappa_{s0}(\hat{p})} \frac{\partial \hat{f}}{\partial \hat{\tau}} \right) \right), \quad \frac{1}{\alpha_k^{\frac{1}{2}}} \frac{\partial \hat{\eta}}{\partial \hat{\tau}} - (\gamma - 1) \frac{\partial \hat{f}}{\partial \hat{\tau}} = \frac{R}{12} \frac{\partial}{\partial \hat{X}} \left( \left( \frac{\hat{\eta}}{\alpha_k^{\frac{1}{2}}} + \hat{f} \right)^3 \frac{\partial^3 \hat{u}}{\partial \hat{X}^3} \right), \tag{2.17}$$

$$\text{at } \hat{X} = 0 \qquad \hat{f} = \frac{\kappa_{s0}(P_0)}{\gamma} \hat{\tau}, \ \hat{u} = \frac{\partial \hat{u}}{\partial \hat{X}} = 0, \ \frac{\partial^2 \hat{u}}{\partial \hat{X}^2} = \frac{P_0}{R}, \tag{2.18}$$

$$\text{as } \hat{X} \to +\infty \qquad \hat{f} \to 0, \ \hat{\eta} \to 1, \tag{2.19}$$

$$\text{at } \hat{\tau} = 0 \qquad \hat{f} = 0, \ \hat{\eta} = 1, \tag{2.20}$$

with $\hat{u} = \hat{\eta}_{\hat{X}\hat{X}}, \hat{p} = R\hat{\eta}_{\hat{X}\hat{X}\hat{X}\hat{X}} = R\hat{u}_{\hat{X}\hat{X}}$, and $\kappa_{s0}$ as defined in (2.14) for argument $\hat{p}$ as well.

In the outer region $\hat{X} = O(1)$ we pose

$$\hat{f} = \hat{f}_0 + o(\alpha_k^{-\frac{1}{4}}), \qquad \hat{u} = \hat{u}_0 + o(1), \qquad \hat{p} = \hat{p}_0 + o(1),$$

with the form of the expansion for $\hat{\eta}$ being determined later after consideration of the inner and third regions. We focus here on the main time-scale $\hat{\tau} = O(1)$, with consideration of earlier times needed to incorporate initial conditions for the nitride mask. At leading order we have

$$\frac{\partial \hat{f}_0}{\partial \hat{\tau}} = \frac{\partial}{\partial \hat{X}}\left(\hat{f}_0 \frac{\partial}{\partial \hat{X}}\left(\frac{1}{\kappa_{s0}(\hat{p}_0)}\frac{\partial \hat{f}_0}{\partial \hat{\tau}}\right)\right), \qquad -(\gamma-1)\frac{\partial \hat{f}_0}{\partial \hat{\tau}} = \frac{R}{12}\frac{\partial}{\partial \hat{X}}\left(\hat{f}_0^3 \frac{\partial^3 \hat{u}_0}{\partial \hat{X}^3}\right), \tag{2.21}$$

$$\text{at } \hat{X} = 0 \qquad \hat{f}_0 = \frac{\kappa_{s0}(P_0)}{\gamma}\hat{\tau},\ \hat{u}_0 = \frac{\partial \hat{u}_0}{\partial \hat{X}} = 0,\ \frac{\partial^2 \hat{u}_0}{\partial \hat{X}^2} = \frac{P_0}{R}, \tag{2.22}$$

$$\text{as } \hat{X} \to +\infty \qquad \hat{f}_0 \to 0, \tag{2.23}$$

$$\text{at } \hat{\tau} = 0 \qquad \hat{f}_0 = 0, \tag{2.24}$$

and $\hat{p}_0 = R\hat{u}_{0\hat{X}\hat{X}}$. In passing, it is worth remarking that when $\kappa_{s0}$ is a constant then this system possesses a similarity solution in the form

$$\hat{f}_0 = \begin{cases} \dfrac{\kappa_{s0}\hat{\tau}}{\gamma}\left(1 - \dfrac{\hat{X}}{\hat{S}(\hat{\tau})}\right)^2, & \hat{X} < \hat{S}(\hat{\tau}), \\ 0, & \hat{X} > \hat{S}(\hat{\tau}), \end{cases} \tag{2.25}$$

and for $\hat{X} < \hat{S}(\hat{\tau})$,

$$\hat{p}_0 = P_0 + \frac{4\gamma(\gamma-1)}{\kappa_{s0}^2\hat{\tau}^2}\left(\left(1 - \frac{\hat{X}}{\hat{S}(\hat{\tau})}\right)^{-3} - 1\right), \qquad \hat{u}_0 = \frac{P_0}{2R}\hat{X}^2 + \frac{4(\gamma-1)}{R\kappa_{s0}^2\hat{\tau}}\left(\frac{(\frac{\hat{X}}{\hat{S}(\hat{\tau})})^3}{\left(1 - \frac{\hat{X}}{\hat{S}(\hat{\tau})}\right)}\right), \tag{2.26}$$

where

$$\hat{S}(\hat{\tau}) = \sqrt{\frac{2\hat{\tau}}{\gamma}}. \tag{2.27}$$

However, of interest here is the case of non constant $\kappa_{s0}$, for which such an analytical solution is not available. The system (2.21)–(2.24) still possesses a weak solution with the necessary smooth continuity conditions of $\hat{f}_0$ and $\hat{f}_{0\hat{X}}$ vanishing at finite location $\hat{X} = \hat{S}(\hat{\tau})$, but which now needs to be determined numerically. It is worth remarking that the scaling $\hat{\eta} = \alpha_k^{\frac{1}{2}}\eta_0$ in (2.17)–(2.20) gives the original system (2.3)–(2.7), (2.9)–(2.10) (with modification (2.13)) but with a scaled rigidity coefficient $\alpha_k^{\frac{1}{2}}R$ and initial, far-field conditions for the nitride being

$$\text{at } \tau = 0 \quad \eta_0 = \delta, \qquad \text{as } X \to +\infty \quad \eta_0 \to \delta, \tag{2.28}$$

with $\delta = \alpha_k^{-\frac{1}{2}}$ in place of (2.11) and (2.12). Thus the large activation volume limit is equivalent to the $\alpha_k = O(1)$ activation volume problem but with large nitride rigidity and vanishingly thin initial pad-oxide. This scaled equivalent formulation may be considered as a suitable regularisation of the leading outer problem (2.21)–(2.24) and used accordingly to generate numerical solutions. Taking $\delta = 0.01, R/\delta = 1$ we may fit the leading term of the expansion (2.42) for $\eta_0$ (which is not fully determined until resolution of the inner and third regions) to give an estimate of the moving front $\hat{S}(\hat{\tau})$. The numerical solution has a least-squares fit $\hat{S} = a\hat{\tau}^b$ with $a = 1.38, b = 0.46$, which compares with $a = (2/\gamma)^{0.5} \approx 0.94, b = 0.5$ of the similarity solution.

In the inner region we write

$$\hat{X} = \hat{S}(\hat{\tau}) + \frac{z}{\alpha_k^{\frac{1}{4}}}, \qquad \hat{f} = \frac{\tilde{f}}{\alpha_k^{\frac{1}{2}}}, \qquad \hat{\eta} = \tilde{\eta}, \qquad \hat{u} = \alpha_k^{\frac{1}{2}}\tilde{u}, \qquad \hat{p} = \alpha_k\tilde{p}, \tag{2.29}$$

so that for $z = O(1)$

$$\frac{1}{\alpha_k^{\frac{1}{4}}}\frac{\partial \tilde{f}}{\partial \hat{\tau}} - \hat{S}'\frac{\partial \tilde{f}}{\partial z} = \frac{\partial}{\partial z}\left(\left(\tilde{\eta} + \tilde{f}\right)\frac{\partial}{\partial z}\left(\frac{1}{\kappa_{s0}(\tilde{p})}\left(\frac{1}{\alpha_k^{\frac{1}{4}}}\frac{\partial \tilde{f}}{\partial \hat{\tau}} - \hat{S}'\frac{\partial \tilde{f}}{\partial z}\right)\right)\right), \tag{2.30}$$

$$\frac{1}{\alpha_k^{\frac{1}{2}}}\left(\frac{\partial \tilde{\eta}}{\partial \hat{\tau}} - (\gamma-1)\frac{\partial \tilde{f}}{\partial z}\right) - \frac{\hat{S}'}{\alpha_k^{\frac{1}{4}}}\left(\frac{\partial \tilde{\eta}}{\partial z} - (\gamma-1)\frac{\partial \tilde{f}}{\partial z}\right) = \frac{R}{12}\frac{\partial}{\partial z}\left(\left(\tilde{\eta} + \tilde{f}\right)^3\frac{\partial^3 \tilde{u}}{\partial z^3}\right), \tag{2.31}$$

where

$$\hat{S}' = \frac{d\hat{S}}{d\hat{\tau}}, \qquad \tilde{u} = \frac{\partial^2 \tilde{\eta}}{\partial z^2}, \qquad \tilde{p} = R\frac{\partial^2 \tilde{u}}{\partial z^2}, \qquad \kappa_{s0}(\tilde{p}) = \begin{cases} 0, & \text{if } \tilde{p} > 0, \\ \kappa_0, & \text{if } \tilde{p} \le 0. \end{cases} \tag{2.32}$$

We pose

$$\begin{aligned}
\tilde{\eta} &\sim a_0(\hat{\tau}) + \alpha_k^{-\frac{1}{20}}(a_1(\hat{\tau}) + b_1(\hat{\tau})z) + \alpha_k^{-\frac{2}{20}}(a_2(\hat{\tau}) + b_2(\hat{\tau})z) + \alpha_k^{-\frac{3}{20}}(a_3(\hat{\tau}) + b_3(\hat{\tau})z) \\
&\quad + \alpha_k^{-\frac{4}{20}}(a_4(\hat{\tau}) + b4(\hat{\tau})z) + \alpha_k^{-\frac{5}{20}}\tilde{M}(z,\hat{\tau}), \\
\tilde{u} &\sim \alpha_k^{-\frac{1}{4}}\tilde{u}_0(z,\hat{\tau}), \qquad \tilde{p} \sim \alpha_k^{-\frac{1}{4}}\tilde{p}_0(z,\hat{\tau}), \qquad \tilde{f} = \tilde{f}_0 + o(1),
\end{aligned} \tag{2.33}$$

with $\tilde{u}_0 = \tilde{M}_{zz}$ and where the $a_i$ and $b_i$ are to be determined (the powers of $\alpha_k^{-\frac{1}{20}}$ arising due to matching with the third region, which is described next). We thus obtain

$$\frac{\partial \tilde{f}_0}{\partial z} = \frac{\partial}{\partial z}\left(\left(\tilde{\eta}_0 + \tilde{f}_0\right)\frac{\partial}{\partial z}\left(\frac{1}{\kappa_{s0}(\tilde{p}_0)}\frac{\partial \tilde{f}_0}{\partial z}\right)\right), \qquad (\gamma-1)\frac{\partial \tilde{f}_0}{\partial z} = \frac{R}{12}\frac{\partial}{\partial z}\left(\left(\tilde{\eta}_0 + \tilde{f}_0\right)^3\frac{\partial^3 \tilde{u}_0}{\partial z^3}\right), \tag{2.34}$$

with $\kappa_{s0}(\tilde{p}_0)$ as defined in (2.32).

In the third region we take

$$z = \alpha_k^{\frac{1}{20}}\xi, \qquad \xi > 0, \qquad \tilde{\eta} = q, \qquad \tilde{u} = \alpha_k^{-\frac{1}{10}}\frac{\partial^2 q}{\partial \xi^2}, \qquad \tilde{p} = \alpha_k^{-\frac{1}{5}}R\frac{\partial^4 q}{\partial \xi^4}, \tag{2.35}$$

with $\xi > 0$ or equivalently $\hat{X} = \hat{S}(\hat{\tau}) + \alpha_k^{-\frac{1}{5}}\xi$. In $\xi = O(1)$ we have $\hat{f}$ exponentially small and

$$\frac{1}{\alpha_k^{\frac{1}{5}}}\frac{\partial q}{\partial \hat{\tau}} - \hat{S}'\frac{\partial q}{\partial \xi} = \frac{R}{12}\frac{\partial}{\partial \xi}\left(q^3\frac{\partial^5 q}{\partial \xi^5}\right). \tag{2.36}$$

Writing

$$q \sim q_0 + \frac{1}{\alpha_k^{\frac{1}{20}}}q_1,$$

we obtain the leading order problem

$$-\hat{S}'\frac{\partial q_0}{\partial \xi} = \frac{R}{12}\frac{\partial}{\partial \xi}\left(q_0^3\frac{\partial^5 q_0}{\partial \xi^5}\right), \tag{2.37}$$

$$\text{at } \xi = 0 \qquad \frac{\partial^2 q_0}{\partial \xi^2} = \frac{\partial^3 q_0}{\partial \xi^3} = \frac{\partial^4 q_0}{\partial \xi^4} = 0, \tag{2.38}$$

$$\text{as } \xi \to +\infty \qquad q_0 = 1, \tag{2.39}$$

where the conditions (2.38) follow from matching to (2.33). The solution is $q_0 = 1$, and matching back into $z = O(1)$ gives $a_0 = 1, b_1 = 0, \lim_{z\to\infty}\tilde{u}_{0zzz} = 0$. Consequently, we obtain in $z = O(1)$,

$$\frac{\partial}{\partial z}\left(\frac{1}{\kappa_{s0}(\tilde{p}_0)}\frac{\partial \tilde{f}_0}{\partial z}\right) = \frac{\tilde{f}_0}{(1+\tilde{f}_0)}, \qquad \frac{\partial^3 \tilde{u}_0}{\partial z^3} = \frac{12(\gamma-1)\hat{S}'}{R}\frac{\tilde{f}_0}{(1+\tilde{f}_0)^3}. \tag{2.40}$$

We remark that we may obtain the following quadrature expression from (2.40),

$$\frac{\partial^2 \tilde{u}_0}{\partial z^2} = \frac{12(\gamma-1)\hat{S}'}{R}\int_{-\infty}^{z}\frac{\tilde{f}_0(\tilde{z})}{(1+\tilde{f}_0(\tilde{z}))^3}d\tilde{z},$$

which has the limiting behaviour as $z \to +\infty$

$$\frac{\partial^2 \tilde{u}_0}{\partial z^2} \to \frac{12(\gamma-1)}{R}S'C, \qquad \text{where} \qquad C = \int_{-\infty}^{\infty}\frac{\tilde{f}_0(\tilde{z})}{(1+\tilde{f}_0(\tilde{z}))^3}d\tilde{z}$$

is a constant. The first order problem in $\xi = O(1)$ is now

$$\begin{aligned}
&-\hat{S}'\frac{\partial q_1}{\partial \xi} \sim \frac{R}{12}\frac{\partial}{\partial \xi}\left(\frac{\partial^5 q_1}{\partial \xi^5}\right), \\
&\text{at } \xi = 0 \qquad \frac{\partial^2 q_1}{\partial \xi^2} = \frac{\partial^3 q_1}{\partial \xi^3} = 0, \ \frac{\partial^4 q_1}{\partial \xi^4} = \frac{12(\gamma-1)}{R}S'C, \\
&\text{as } \xi \to +\infty \qquad q_1 = 0,
\end{aligned}$$

with solution

$$q_1 = \frac{(\gamma-1)\omega C}{(\cos(2\pi/5)+\cos(\pi/5))}\left(\cos(\pi/5)e^{-\omega\xi} + \cos(\omega\xi\sin(2\pi/5))e^{-\omega\xi\cos(2\pi/5)}\right), \qquad \omega = \left(\frac{12\hat{S}'}{R}\right)^{\frac{1}{5}}. \tag{2.41}$$

Matching back into $z = O(1)$ gives

$$a_1 = \frac{(\gamma-1)\omega C(1+\cos(\pi/5))}{(\cos(2\pi/5)+\cos(\pi/5))}, \qquad b_1 = -(\gamma-1)\omega^2 C.$$

In the outer region $\hat{X} = O(1)$ we finally have

$$\hat{\eta} \sim \alpha_k^{-\frac{3}{20}} \left(\hat{X} - \hat{S}\right) b_2(\hat{\tau}) + \alpha_k^{-\frac{1}{10}} \left(\hat{X} - \hat{S}\right) b_3(\hat{\tau}) + \alpha_k^{-\frac{1}{20}} \left(\hat{X} - \hat{S}\right) b_4(\hat{\tau}) + M(\hat{X}, \hat{\tau}), \tag{2.42}$$

where $\hat{u} = M_{\hat{X}\hat{X}}$, which determines the expansion for $\hat{\eta}$ in the $\hat{X} = O(1)$ region.

We may summarise the main regions with the pressure scalings as follows,

$$\text{in } X = O(\alpha_k^{\frac{1}{4}}) \quad p = O(\alpha_k^{-1}), \qquad \text{in } X = S(\tau) + O(1) \quad p = O(\alpha_k^{-\frac{1}{4}}), \qquad \text{in } X = S(\tau) + O(\alpha_k^{\frac{1}{20}}) \quad p = O(\alpha_k^{-\frac{1}{4}}),$$

where $S(\tau) = \alpha_k^{\frac{1}{4}} \hat{S}(\tau/\alpha_k^{\frac{1}{2}})$ is a moving front that marks the lateral extent of oxidation under the nitride mask. This front is not obtained until significantly large times $\tau = O(\alpha_k^{\frac{1}{2}})$ and follows a power-law behaviour in time, not too different from the similarity solution (2.27) (for which $S(\tau) = \sqrt{2\tau/\gamma}$ ). The largest pressures are obtained at the front and ahead of it, the activation energy being large $\alpha_k p = O(\alpha_k^{\frac{3}{4}})$. The reaction is thus switched off in the these regions where the pressure is positive and only retained where the pressure is negative. The oscillatory nature of the pressure thus gives an on-off behaviour to the reaction with lateral extent under the mask.

Before leaving the bird's beak problem, we remark that the generalised lubrication equation (2.9) simplifies in the limits of small and large rigidity. These limits are discussed briefly in Appendix B for the $\alpha_k = o(1/\epsilon)$ case, giving rise to particular novel forms of nonlinear evolution equations.

# 3 Cylindrical and spherical oxidation

Oxidation of cylindrical and spherical structures are higher-dimensional situations in which quantitative effects of stress-dependent parameters can be studied. Results in the stress independent cases for cylindrical geometries have been obtained by King [20] and Wilson and Marcus [42]. The stress dependent case in a cylindrical geometry was originally considered by Kao et al. [16], with both cylindrical and spherical cases considered in Evans [10]. Throughout we treat the silicon as rigid, though this assumption will of course cease to be valid if the stresses in the silicon become too large. A pressure dependent diffusion coefficient will be retained throughout, to determine its influence.

The non-dimensionalised governing equations that we consider are

$$\nabla.(D_s \nabla c) = 0, \qquad \nabla.\mathbf{v} = 0, \qquad 0 = -\nabla p + \nabla^2 \mathbf{v},$$

corresponding to quasi-steady diffusion of oxidant and the creeping flow equations for the oxide. In a structure with cylindrical symmetry, introducing cylindrical polar coordinates $(r, \theta, z)$, leads (since a pressure dependent diffusion coefficient $D_s$ will be a function of time only) to the solutions

$$c = a_1(t) \ln r + a_2(t), \qquad v_r = \frac{a_3(t)}{r}, \qquad v_\theta = 0, \qquad v_z = 0,$$

where $a_i(t), i = 1, 2, 3$ are functions to be determined. The stress components are consequently given by

$$\sigma_{rr} = -p - 2\frac{a_3(t)}{r^2}, \qquad \sigma_{\theta\theta} = -p + 2\frac{a_3(t)}{r^2}, \qquad \sigma_{r\theta} = 0, \qquad p = p(t),$$

where $p(t)$ is also to be determined. For structures with spherical symmetry, introducing spherical polar coordinates $(r, \theta, \phi)$, we have solutions of the form

$$c = \frac{b_1(t)}{r} + b_2(t), \qquad v_r = \frac{b_3(t)}{r^2}, \qquad v_\theta = 0, \qquad v_\phi = 0,$$

where the $b_i(t), i = 1, 2, 3$ are functions to be determined. The stress components in this case are given by

$$\sigma_{rr} = -p - \frac{4b_3(t)}{r^3}, \quad \sigma_{\theta\theta} = \sigma_{\phi\phi} = -p + \frac{2b_3(t)}{r^3}, \quad \sigma_{r\theta} = \sigma_{r\phi} = \sigma_{\theta\phi} = 0, \quad p = p(t),$$

with $p(t)$ again to be determined.

## 3.1 Silicon cylinders and spheres

We consider first the oxidation of silicon cylinders and spheres as examples of convex structures. In both cases we denote the $Si/SiO_2$ interface by $r = d(t)$ and the $SiO_2$/gas by $r = b(t)$, with initial values $d(0) = d_0 < b(0) = b_0$ at $t = 0$. The initial oxide thickness is used for nondimensionalising lengths, so that $b_0 = d_0 + 1$. The boundary conditions we take are

$$\text{on } r = d \qquad D_s \frac{\partial c}{\partial r} = k_s c, \;\; v_r = \frac{\gamma - 1}{\gamma} D_s \frac{\partial c}{\partial r}, \;\; \gamma \dot{d} = -D_s \frac{\partial c}{\partial r}, \tag{3.1}$$

$$\text{on } r = b \qquad D_s \frac{\partial c}{\partial r} = H(1-c), \;\; \dot{b} = v_r, \;\; \sigma_{rr} = 0. \tag{3.2}$$

In the cylindrical case we therefore obtain

$$c = \frac{Hk_s\, bd\, \ln(r/d) + HD_s b}{Hk_s\, db\, \ln\left(\frac{b}{d}\right) + HD_s b + D_s k_s d} \tag{3.3}$$

$$v_r = \left(\frac{\gamma - 1}{\gamma}\right) \frac{Hk_s\, db}{r\left(Hk_s\, db\, \ln\left(\frac{b}{d}\right) + HD_s b + D_s k_s d\right)}, \tag{3.4}$$

$$\gamma \dot{d} = -\frac{Hk_s\, b}{Hk_s\, db\, \ln\, b/d + HD_s b + D_s k_s d}, \tag{3.5}$$

$$\dot{b} = \frac{\gamma - 1}{\gamma} \frac{Hk_s\, d}{Hk_s\, db\, \ln\left(\frac{b}{d}\right) + HD_s b + D_s k_s d}, \tag{3.6}$$

where $(\gamma - 1) d\dot{d} + b\dot{b} = 0$ and therefore

$$(\gamma - 1) d^2 + b^2 = (\gamma - 1) d_0^2 + b_0^2, \tag{3.7}$$

as would be expected by conservation of mass. The stress components in the oxide are

$$\sigma_{rr} = 2b\dot{b}\left(\frac{1}{b^2} - \frac{1}{r^2}\right), \qquad \sigma_{\theta\theta} = 2b\dot{b}\left(\frac{1}{b^2} + \frac{1}{r^2}\right), \qquad p = -2\frac{\dot{b}}{b}. \tag{3.8}$$

We remark that the effect of the diffusion coefficient can be removed by suitable redefinition of the parameters $k_s$ and $H$ (the latter now becoming time-dependent). Further, since $p < 0$, the diffusion coefficient of dimensional form (1.2) would take its stress free value $D_s = 1$ in such geometries and thus have no influence from the stress-independent case. This is consistent with the findings of [39] at convex corners.

In the case of a constant reaction coefficient ($k_s = k_0$), (3.5) and (3.6) can be integrated to give

$$\frac{d}{k_0} - \frac{b}{H(\gamma - 1)} - \frac{1}{2(\gamma - 1)} b^2 \ln b - \frac{1}{2} d^2 \ln d = -\frac{t}{\gamma} + \frac{d_0}{k_0} - \frac{b_0}{H(\gamma - 1)} - \frac{1}{2(\gamma - 1)} b_0^2 \ln b_0 - \frac{1}{2} d_0^2 \ln d_0. \tag{3.9}$$

The cylinder is thus completely oxidised ($d = 0$) at finite time $t^*$ given by

$$\frac{t^*}{\gamma} = \frac{d_0}{k_0} - \frac{1}{2} d_0^2 \ln d_0 + \frac{(b_e - b_0)}{H(\gamma - 1)} + \frac{1}{2(\gamma - 1)} \left(b_e^2 \ln b_e - b_0^2 \ln b_0\right), \qquad b_e = \left((\gamma - 1) d_0^2 + b_0^2\right)^{\frac{1}{2}}, \tag{3.10}$$

the solution being physically meaningless for $t > t^*$. In the limit of complete oxidation, we have

$$\dot{b} \sim \frac{\gamma - 1}{\gamma} \frac{k_0 d}{b} \qquad \text{as } d \to 0,$$

which gives the prediction of unbounded stresses on the $Si/SiO_2$ interface.

The stress-dependent case gives a qualitatively different behaviour. We have on the $Si/SiO_2$ interface $r = d$ that

$$\sigma_{nn} = \sigma_{rr}(d) = 2b\dot{b}\left(\frac{1}{b^2} - \frac{1}{d^2}\right), \tag{3.11}$$

and adopting the exponential dependence (1.6), then (3.5) gives the asymptotic behaviour

$$\dot{d} \sim -\frac{k_0}{\gamma} \exp\left(2(\gamma - 1)\alpha_k \frac{\dot{d}}{d}\right) \qquad \text{as } d \to 0. \tag{3.12}$$

This implies that the time for complete oxidation is no longer bounded with instead the hyper-exponential large-time behaviour of the form

$$d \sim e^{-B_1 e^{t/(2(\gamma-1)\alpha_k)}} \qquad \text{as } t \to \infty,$$

CylOx.pdf

Figure 4: Geometry for oxidation of silicon cylinders/spheres and cavities.

for some positive constant $B_1$, the build up of compressive stress thus leading to very slow oxidation at large times. Numerical solution of (3.5)–(3.7) may be obtained using the implicit Matlab solver ode15i. Plots in Figure 5 illustrate the already remarked qualitative difference in behaviours that are obtained in the stress independent and dependent cases of the reaction coefficient. Results for the evolution of the radii and their speed are shown in Figure 5 for a representative case $d_0 = 10$. Plots for the stress $\sigma_{rr}(d)$ and pressure are similar to the $\dot{d}$ and $\dot{b}$ curves in 5(A2). Further plots for a greater range of initial radii can be found in [10], which are qualitatively similar. Figure 5 (B1) and (B2) quantify the effect of the reaction coefficient on the oxide thickness at the stress-independent complete oxidation time $t^*$ from (3.10) and time to saturation (arbitrarily defined to be time when $d = 10^{-3}$) for different initial radii.

It is worth remarking that in the case of large initial radii, we recover the Deal-Grove solution, the surfaces being planar at leading order. The details of the asymptotics in this case are given in Appendix B.

For spherical oxidation, we have the corresponding results

$$c = \frac{Hb^2}{(Hk_s db(b-d) + k_s D_s d^2 + HD_s b^2)} \left( D_s + k_s d - k_s \frac{d^2}{r} \right), \tag{3.13}$$

$$v_r = \left( \frac{\gamma - 1}{\gamma} \right) \frac{Hk_s d^2 b^2}{r^2 \left( Hk_s db(b-d) + k_s D_s d^2 + HD_s b^2 \right)}, \tag{3.14}$$

$$\gamma \dot{d} = -\frac{Hk_s\, b^2}{Hk_s db(b-d) + k_s D_s d^2 + HD_s b^2}, \tag{3.15}$$

$$\dot{b} = \left( \frac{\gamma - 1}{\gamma} \right) \frac{Hk_s\, d^2}{Hk_s db(b-d) + k_s D_s d^2 + HD_s b^2}, \tag{3.16}$$

with

$$b^3 + (\gamma - 1)d^3 = b_0^3 + (\gamma - 1)d_0^3.$$

The stress components in the oxide are now

$$\sigma_{rr} = 4\, b^2 \dot{b} \left( \frac{1}{b^3} - \frac{1}{r^3} \right), \quad \sigma_{\theta\theta} = \sigma_{\phi\phi} = 2b^2 \dot{b} \left( \frac{1}{r^3} - \frac{2}{b^3} \right), \quad p = -4\frac{\dot{b}}{b}, \tag{3.17}$$

and again since $p < 0$ (due to $\dot{b} > 0$) the diffusion coefficient would take its stress free value $D_s = 1$.

In the stress-independent reaction coefficient case we have

$$\frac{d}{k_0} - \frac{b}{H(\gamma - 1)} + \frac{1}{2}d^2 + \frac{b^2}{2(\gamma - 1)} = -\frac{t}{\gamma} + \frac{d_0}{k_0} - \frac{b_0}{H(\gamma - 1)} + \frac{1}{2}d_0^2 + \frac{b_0^2}{2(\gamma - 1)},$$

FigCyl.pdf

Figure 5: Oxidation of a silicon cylinder. (A1) and (A2) show numerical solution for the evolution of the radii and their speeds ($\dot{b} > 0, \dot{d} < 0$) in the particular case of initial radii $d_0 = 10, b_0 = 11$, obtained by solving (3.5)–(3.7) with Matlab solver ode15i (error tolerances AbsTol= $10^{-6}$, RelTol= $10^{-3}$). Parameter values are $\gamma = 2.27, k_0 = 1, H = 1, D_s = 1$ with $\alpha_k = 0$ in the stress independent case and $\alpha_k = 1, 10, 100, 1000$ for the stress dependent case. (B1) and (B2) show the oxide thickness at the stress-independent complete oxidation time $t^*$ and time to saturation (when $d = 10^{-3}$) for different initial radii $d_0$.

with complete oxidation at finite time $t^*$ given by

$$\frac{t^*}{\gamma} = \frac{d_0}{k_0} + \frac{1}{2}d_0^2 + \frac{(b_e - b_0)}{H(\gamma - 1)} + \frac{(b_0^2 - b_e^2)}{2(\gamma - 1)}, \qquad b_e = \left(b_0^3 + (\gamma - 1)d_0^3\right)^{\frac{1}{3}}.$$

As in the cylindrical case, stresses on the $Si/SiO_2$ interface become unbounded as complete oxidation is approached.

In the stress-dependent case, the normal stress on the $Si/SiO_2$ boundary is

$$\sigma_{nn} = \sigma_{rr}(d) = 4b^2\dot{b}\left(\frac{1}{b^3} - \frac{1}{d^3}\right),$$

and we have the asymptotic behaviours

$$\sigma_{nn} \sim 4(\gamma - 1)\frac{\dot{d}}{d}, \quad p \sim 4(\gamma - 1)\frac{d^2\dot{d}}{(b_0^3 + (\gamma - 1)d_0^3)} \qquad \text{as } d \to 0.$$

Taking the exponential functional dependence (1.6), (3.15) gives

$$\dot{d} \sim -\frac{k_0}{\gamma}\exp\left(4(\gamma - 1)\alpha_k\frac{\dot{d}}{d}\right) \qquad \text{as } d \to 0 \tag{3.18}$$

and the time for complete oxidation is now unbounded with the large-time behaviour

$$\ln d \sim -B_2 e^{t/4(\gamma-1)\alpha_k} \qquad \text{as } t \to \infty,$$

for some positive constant $B_2$. It is noteworthy that the controlling asymptotic behaviour (3.18) is similar to that in the cylindrical case (3.12) due to the similar dependence of the limiting behaviour of the normal stress on the $Si/SiO_2$ interface location in both geometries.

The results for oxidation inhibition of silicon in the stress-dependent spherical case, are in qualitative agreement with experimentally observed results of Okada and Lijima [26], and may provide an explanation of the types of silicon tips observed experimentally by Marcus and Sheng [25]. These results suggest that a stress-dependent reaction coefficient will be important in regions of high curvature, particularly for convex structures, with a stress-dependent diffusion coefficient being less so if it has a pressure dependence.

## 3.2 Silicon cavities

We now consider the oxidation of silicon cavities, as examples of concave structures. Again, we denote the $Si/SiO_2$ interface by $r = d(t)$ and the $SiO_2/gas$ interface by $r = b(t)$ with initial values $d(0) = d_0 > b(0) = b_0$, $b_0 = d_0 - 1$ at $t = 0$. The boundary conditions are now

$$\begin{aligned} &\text{on } r = d \qquad && -D_s\frac{\partial c}{\partial r} = k_s c, \;\; v_r = \frac{\gamma-1}{\gamma} D_s \frac{\partial c}{\partial r}, \;\; \gamma\dot{d} = -D_s\frac{\partial c}{\partial r}, \\ &\text{on } r = b && -D_s\frac{\partial c}{\partial r} = H(1-c), \;\; \dot{b} = v_r, \;\; \sigma_{rr} = 0. \end{aligned}$$

We remark that we may deduce the results from the convex case by changing the sign of H and $k_s$ in the results of section 3.1.

In the cylindrical case we obtain

$$c = \frac{Hk_s db\ln(r/d) - HD_s b}{Hk_s db\ln(b/d) - HD_s b - k_s D_s d}, \tag{3.19}$$

$$v_r = \left(\frac{\gamma-1}{\gamma}\right)\frac{Hk_s db}{r\left(Hk_s db\ln\left(\frac{b}{d}\right) - HD_s b - k_s D_s d\right)}, \tag{3.20}$$

$$\gamma\dot{d} = -\frac{Hk_s b}{Hk_s db\ln\left(\frac{b}{d}\right) - HD_s b - k_s D_s d}, \tag{3.21}$$

$$\dot{b} = \left(\frac{\gamma-1}{\gamma}\right)\frac{Hk_s d}{Hk_s db\ln\left(\frac{b}{d}\right) - HD_s b - k_s D_s d}, \tag{3.22}$$

with

$$(\gamma-1)d^2 + b^2 = (\gamma-1)d_0^2 + b_0^2,$$

and the stress components are given in (3.8). Since $p > 0$ and $\sigma_{nn} = \sigma_{rr}(d) < 0$, then the stress dependent reaction and diffusion coefficients are expected to vary from their stress free values.

In the stress-independent case we have

$$\frac{d}{k_0} - \frac{b}{H(\gamma-1)} + \frac{1}{2(\gamma-1)}b^2\ln b + \frac{1}{2}d^2\ln d = \frac{t}{\gamma} + \frac{d_0}{k_0} - \frac{b_0}{H(\gamma-1)} + \frac{b_0^2}{2(\gamma-1)}\ln b_0 + \frac{1}{2}d_0^2\ln d_0,$$

and the cavity becomes completely filled ($b = 0$) in finite time $t = t_c^*$ given by

$$\frac{t_c^*}{\gamma} = \frac{(d_e - d_0)}{k_0} + \frac{1}{2}\left(d_e^2\ln d_e - d_0^2\ln d_0\right) + \frac{b_0}{H(\gamma-1)} - \frac{1}{2(\gamma-1)}b_0^2\ln b_0, \qquad d_e = \left(d_0^2 + \frac{b_0^2}{\gamma-1}\right)^{\frac{1}{2}}.$$

As $b \to 0$ the stresses $\sigma_{rr}$ and $\sigma_{\theta\theta}$ become unbounded throughout the oxide, rather than just at the $Si/SiO_2$ interface as in the silicon cylinder case.

We contrast this with the stress-dependent case, in which

$$\sigma_{nn} = \sigma_{rr}(d) \sim 2\frac{\dot{b}}{b}, \quad p \sim -2\frac{\dot{b}}{b} \qquad \text{as } b \to 0.$$

Considering first, the effect of a stress-dependent reaction coefficient only (and taking $D_s = 1$), then (3.22) gives the asymptotic behaviour

$$\dot{b} \sim -\frac{\gamma-1}{\gamma}\frac{d}{b}\exp\left(2\alpha_k\frac{\dot{b}}{b}\right) \qquad \text{as } b \to 0, \tag{3.23}$$

and thus, as in the convex case, complete filling of the cavity now occurs in unbounded time, with

$$\ln b \sim -B_3 e^{t/2\alpha_k} \qquad \text{as } \ t \to \infty,$$

for some positive constant $B_3$. However, also allowing the diffusion coefficient to vary from its stress free value, implies that complete filling of the cavity occurs in finite time where

$$b \ln b \, \dot{b} \sim \frac{\gamma - 1}{\gamma} \qquad \text{as } b \to 0,$$

and thus

$$b^2 \ln b \sim 2 \left( \frac{\gamma - 1}{\gamma} \right) (t_c - t) \qquad \text{as } t \to t_c^-, \tag{3.24}$$

where $t_c$ is the time at which the cavity is filled. These two contrasting cases are illustrated numerically in Figure 6. Numerical solution of (3.21)–(3.22) is again obtained using the implicit Matlab solver ode15i. Results for the evolution of the oxide thickness are given in Figure 6(A1) and (A2) for a stress-dependent reaction coefficient only. (A1) shows the slowing of growth of the oxide thickness as the activation volume increases for a representative initial radius $b_0 = 10$. (A2) gives the oxide thickness at the stress-independent complete oxidation time $t_c^*$ for a range of initial radii. The reduction in oxide growth is significant for the larger $\alpha_k$ values. In contrast, 6(B1) and (B2) show the effect of both stress-dependent reaction and diffusion coefficients. Complete oxidation time in the stress-dependent case is now finite, as predicted by (3.24). (B1) shows that this reduces as the activation volume increases. This is mainly due to larger initial speeds of the radii as $\alpha_k$ increases. If stress-free initial speeds are used in the stress-dependent cases, then the finite oxidation times are longer than in the stress-free case as would be expected. (B2) shows the variation of the saturation time $t_c$ with a range of initial radii, for selected activation volumes.

For the spherical cavity case, qualitatively similar results are obtained. Expressions for the concentration $c$, radial velocity $v_r$ and surface speeds can be deduced from the (3.13)–(3.16) in the spherical case by simply changing the sign of $H$ and $k_s$ in those expressions. The stress components are again as given in (3.17). Similar to the cylindrical cavity case, have $p > 0, \sigma_{nn} = \sigma_{rr}(d) < 0$, indicating that both reaction and diffusion coefficients will vary from their stress free value.

The stress-independent case gives

$$\frac{d}{k_0} - \frac{b}{H(\gamma - 1)} - \frac{1}{2} d^2 - \frac{b^2}{2(\gamma - 1)} = \frac{t}{\gamma} + \frac{d_0}{k_0} - \frac{b_0}{H(\gamma - 1)} - \frac{1}{2} d_0^2 - \frac{b_0^2}{2(\gamma - 1)},$$

with complete filling of the spherical cavity ($b = 0$) in finite time $t = t_s^*$ given by

$$\frac{t_s^*}{\gamma} = \frac{(d_e - d_0)}{k_0} + \frac{1}{2}(d_0^2 - d_e^2) + \frac{b_0}{H(\gamma - 1)} + \frac{b_0^2}{2(\gamma - 1)}, \qquad d_e = \left( d_0^3 + \frac{b_0^3}{\gamma - 1} \right)^{\frac{1}{3}}.$$

Since the stresses become unbounded throughout the oxide in these concave structures as the limit of complete oxidation is reached, a stress-dependent diffusion coefficient would be expected to have comparable oxide-growth retardation effects as the stress-dependent reaction coefficient.

In the stress-dependent case with constant diffusion coefficient ($D_s \equiv 1$), the time for the complete filling of the spherical cavity is now unbounded with the behaviour,

$$b^2 \dot{b} \sim - \left( \frac{\gamma - 1}{\gamma} \right) d k_0 \exp \left( 4 \alpha_k \frac{\dot{b}}{b} \right) \qquad \text{as } b \to 0,$$

and hence

$$\ln b \sim -B_4 e^{3t/4\alpha_k} \qquad \text{as } \ t \to \infty,$$

for some constant $B_4 > 0$. If the diffusion coefficient is also allowed to vary from its stress free value as well, then the spherical hole fills in finite time $t_s$,

$$b^2 \dot{b} \sim - \left( \frac{\gamma - 1}{\gamma} \right) \qquad \text{as } b \to 0,$$

and thus

$$b^3 \sim 3 \left( \frac{\gamma - 1}{\gamma} \right) (t_s - t) \qquad \text{as } t \to t_s^-,$$

where $t_s$ is now the time at which the spherical cavity is filled.

FigCavNew.pdf

Figure 6: Oxidation of a silicon cavity. Numerical solution of (3.21)–(3.22) with Matlab solver ode15i and error tolerances AbsTol= $10^{-6}$, RelTol= $10^{-3}$. (A1) and (A2) consider a stress-dependent reaction coefficient only, whilst (B1) and (B2) include the additional effect of a stress-dependent diffusion coefficient. Parameter values are $\gamma = 2.27, k_0 = 1, H = 1$. In (A1) and (A2) $\alpha_d = 0$, whilst for (B1) and (B2) $\alpha_d = 4\alpha_k$ for use of $D_s$ in (1.6). (A1) and (B1) show the growth of oxide thickness for an initial starting radius of $b_0 = 10$. (A2) gives the oxide thickness at the stress-independent complete oxidation time $t_c^*$. (B2) is the complete oxidation times $t_c$ for a range of initial radii.

# 4 Discussion

The main objectives in modelling the isolation oxidation of silicon is to predict the lateral extent of oxidation under the nitride mask and the stresses within the silicon oxide. Both aspects become increasingly important as device dimensions shrink deep into the submicron range. The results of Section 2 show the significant effect that a stress dependent reaction coefficient has on reducing both the lateral extent of oxidation and the stresses within the silicon oxide. The former feature allows a larger region to be available for active device location, whilst the latter preserves crystal integrity of the silicon preventing dislocations from forming. Thus as packing density of integrated circuits in VLSI technology increases, incorporation of stress dependent features in the model are essential for software to give accurate predictions for use in process CAD.

An immediate extension of this work is to the consideration of 3D LOCOS structures. Three typical mask structures worthy of investigation are the so called hole, island and line structures (see [41]). Again, the behaviour of the bird's beak length and oxide flow stresses are the key features to ascertain in understanding the three-dimensional behaviour of the oxide growth. The effect at the corners of the nitride mask will be of particular interest.

A future aspect of the modelling that needs addressing is that of consideration of a viscoelastic oxide. This will increase the range of processing conditions for which the model can be used. However, there are several

complications in developing a fully nonlinear flow model, the most significant being the continual creation of new silicon oxide through the interface reaction, as well as choice of a suitable viscoelastic constitutive law. Finally, we remark that the viscous flow model as presented here is valid for temperatures above $960^o$. Incorporating a pressure-dependent viscosity of the form (1.3), modifies the generalised lubrication equation (2.9) to

$$\frac{\partial \eta_0}{\partial \tau} - (\gamma - 1)\frac{\partial f_0}{\partial \tau} = \frac{R}{12}\frac{\partial}{\partial X}\left((\eta_0 + f_0)^3 \frac{1}{\mu_s}\frac{\partial^5 \eta_0}{\partial X^5}\right),$$

with $\mu_s$ a dimensionless viscosity function of the leading order pressure $p_0 = R\eta_{0XXXX}$. This equation is also relevant if the oxide is treated as a power-law fluid, with $\mu_s$ now an appropriate power of the leading order pressure gradient $p_{0X} = R\eta_{0XXXXX}$.

Finally, it is worth remarking that the forms of the lubrication equation for small and large nitride rigidity (see (B.25) and (B.28) in Appendix B) admit travelling wave solutions with varying speed in the stress independent case [21, 22]. Examining if such solutions play a role for the stress-dependent forms of these equations, particularly with more general mask edge conditions, is an aspect which merits further attention.

# References


[1] V. Agache, R. Ringot, P. Bigotte, V. Senez, B. Legrand, L. Buchaillot and D. Collard, *Modeling and experimental validation of sharpening mechanism based on themral oxidation for fabrication of ultra-sharp siliclon nanotips.* IEEE Trans. NanoTechnology, 4 (2005), pp. 548-556.

[2] T. Akiyama, K. Kawamoto, H. Kageshima, M. Uematsu, K. Nakamura and T. Ito, *A first-principles study of $O_2$ incorporatin and its diffusion in compressively strained high-density silicon oxides*, Thin Solid Films, 508 (2006), pp. 311-314.

[3] T. Akiyama, H. Kageshima, M. Uematsu and T. Ito, *Stress-dependence of oxidation reaction at $SiO_2/Si$ interfaces during silicon thermal oxidation*, Jap. J. Appl. Phys., 47 (2008), pp. 7089-7093.

[4] J.A. Appels, E. Kooi, M.M. Paffen, J.J.H. Schatorjé and W.H.C.G. Verkuylen, *Local oxidation of silicon and its application in semiconductor-device technology*, Phillips Res. Rep., 25 (1970), pp. 118-132.

[5] P.W. Bridgman, *The physics of high pressure*, London: G. Bell and Sons, Ltd., 1949.

[6] A. Bryant, W. Hansch and T. Mii *Characteristics of CMOS device isolation for the ULSI age*, IEDM Tech. Dig., 671 (1994), pp. 28.1.1–28.1.4.

[7] H. Coffin, C. Bonafos, S. Schamm, N. Cherkashin, G. Ben Assayag and A. Claverie, *Oxidation of Si nanocrystals fabricated by ultralow-energy ion implantation in thin $SiO_2$ layers*, J. Appl. Phys., 99 (2006), pp. 044302-1–044302-9.

[8] D. Collard, B. Baccus and V. Senez *Psuedo-analytical modelling of stress dependent silicon oxidation*, Micro. Eng., 19 (1992), pp. 491–494.

[9] B.E. Deal and A.S. Grove, *General relationship for the thermal oxidation of silicon*, J. Appl. Phys., 36 (1965), pp. 3770–3778.

[10] J.D. Evans, *Control of stress fields in silicon device fabrication*, D.Phil. Thesis, Oxford University, Oxford, 1992.

[11] J.D. Evans, M. Vynnycky and S.P. Ferro, *Oxidation induced stresses in the isolation oxidation of silicon.* J. Eng. Math. 38 (2000), pp. 191–218.

[12] J. Fan, R. Huang, R. Wang, Q. Xu, Y. Ai, X. Xu, M. Li and Y. Wang, *Two-dimensional self-limiting wet oxidation of silicon nanowires: Experiments and modeling.* IEEE Trans. Electron Dev. 60 (2013), pp. 2747–2753.

[13] X-L. Han, G. Larrieu and C. Krzeminski, *Modelling and engineering of stress based controlled oxidation effects for silicon nanostructure patterning.* NanoTechnology 24 (2013), pp. 495301 1–14.

[14] S.V. Kalinin and A.V. Egorkin, *Two-dimensional simulation of the silicon nanowires thinning effect during the thermal oxidation.* IEEE 16th Int. Conf. Micro/NanoTechnol. & Electron Dev. EDM 60 (2015), pp. 24–26.

[15] S.V. Kalinin and A.V. Egorkin, *Two-dimensional thermal oxidation of nonplanar silicon surfaces.* Russian Microelectronics 44 (2015), pp. 114–126.

[16] D.-B. Kao, J.P. McVittie, W.D. Nix and K.C. Saraswat, *Two-dimensional thermal oxidation of silicon – I. Experiments*, IEEE Trans. Electron Dev. ED- 34 (1987), pp. 1008–1017.

[17] D.-B. Kao, J.P. McVittie, W.D. Nix and K.C. Saraswat, *Two-dimensional thermal oxidation of silicon – II. Modeling stress effects in wet oxides*, IEEE Trans. Electron Dev. ED-35 (1988), pp. 25–37.

[18] L.E. Katz, *Oxidation*, in VLSI technology. Second Ed., S.M. Sze (editor), McGraw-Hill, New York, pp. 98–140, 1988.

[19] I. Kim, T-E. Park, K-Y. Lee, R. Ha, B-H. Kim, Y-C. Chung, K-R. Lee and H-J. Choi, *Interfacial reaction-dominated full oxidation of 5nm diameter silicon nanowires*, J. Appl. Phys., 112 (2012), pp. 094308-1–094308-6.

[20] J.R. King, *Mathematical aspects of semiconductor process modelling*, D.Phil. Thesis, Oxford University, Oxford, 1986.

[21] J.R. King, *The isolation oxidation of silicon*, SIAM J. Appl. Math., 49 (1989), pp. 264–280.

[22] J.R. King, *The isolation oxidation of silicon: the reaction controlled case*, SIAM J. Appl. Math. 49 (1989), pp. 1064–1080.

[23] C.D. Krzeminski, X-L. Han and G. Larrieu, Understanding of the retarded oxidation effects in sililcon nanostructures. *Appl. Phys. Letts.* **100** (2012), pp. 263111-1–263111-4.

[24] J.H. Li and D.R. Uhlman, *The flow of glass at high stress levels. I. Non Newtonian behaviour of homo* $0.08Rb_2O \cdot 0.92\ SiO_2$ *glasses*, J. Non-Crystalline Solids 3 (1970), pp. 127–147.

[25] R.B. Marcus and T.T. Sheng, *The oxidation of shaped silicon surfaces*, J. Electrochem. Soc. 129 (1982), pp. 1278–1282.

[26] R. Okada and S. Lijima, Oxidation property of silicon small particles. *Appl. Phys. Lett.* **58** (1991), pp. 1662–1663.

[27] W. Paul and D.M. Warschauer, Eds., *Solid under pressure*, New York: McGraw-Hill, 1963.

[28] V. Pott, K.E. Moselund, D. Bouvet, L. De Michielis, A.M. Ionescu, Fabrication and characterization of Gate-all-around sililcon nanowires on bulk silicon. *IEEE Trans. NanoTechnology* **7** (2008), pp. 733–744.

[29] R.J. Powell, J.R. Ligenza and M.S. Schneider, *Selective oxidation of silicon in low-temperature high-pressure steam*, IEEE Trans. Electron Dev. ED-21 (1974), pp. 636–640.

[30] A. Seidl, V. Huber and E. Lorenz (1988). Implementation of models for stress-reduced oxidation into 2-D simulator. pp.277–288 of Simulation of semiconductor devices and processes *Vol. 3*, edited by G. Baccarani and M. Rudan, Tecnoprint, 1988.

[31] V. Senez, T. Hoffman and A. Tixier, *Calibration of a two-dimensional numerical model for the optimization of LOCOS-type isolations by response surface methodology*, IEEE Trans. Semi. Manuf. 13 (2000), pp. 416–426.

[32] V. Senez, D. Collard, B. Baccus, M. Brault and J. Lebailly, *Analysis and application of a viscoelastic model for silicon oxidation*, J. Appl. Phys. 76 (1994), pp. 3285–3296.

[33] D. Shir, B.Z. Liu, A.M. Mohammad, K.K. Lew and S.E. Mohney, *Oxidation of silicon nanowires*, J. Vac. Sci. Technol. B (2006), pp. 1333–1336.

[34] P. Sutardja and W.G. Oldham, *Modeling of stress effects in silicon oxidation*, IEEE Trans. Electron Dev. ED-36(1989), pp. 2415–2421.

[35] S.M. Sze, *VLSI Technology*, McGraw-Hill, 2nd edition, 1988.

[36] Y. Tamaki, T. Kure, T. Shiba and H. Higuchi *U-Groove isolation technology for high density bipolar LSI's*, Jpn. J. Appl. Phys. 21 (1982), pp. 37–40.

[37] T. Uchida, M. Fujinaga, N. Kotani, S. Kawazu and H. Miyoshi *Stable solution method for viscoelastic oxidation including stress-dependent viscosity*, Jpn. J. Appl. Phys. 35 (1996), pp. 4265–4273.

[38] T. Uchida and K. Nishi *Formulation of a viscoelastic stress problem using analytical integration and its application to viscoelastic oxidation simulation*, Jpn. J. Appl. Phys. 12 (2001), pp. 6711–6719.

[39] H. Umimoto, S. Odanaka and I. Nakao, *Numerical simulation of stress-dependent oxide growth at convex and concave corners of trench structures*, IEEE Electron Dev. Lett. 10 (1989), pp. 330–332.

[40] H. Umimoto, s. Odanaka, I. Nakao and H. Esaki, *Numerical modeling of nonplanar oxidation coupled with stress effects*, IEEE Trans. Computer–Aided Design. 8 (1989), pp. 599–607.

[41] H. Umimoto and S. Odanaka, *Three-dimensional numerical simulation of local oxidation of silicon*, IEEE Trans. Electron Dev. 38 (1991), pp. 505–511.

[42] L.O. Wilson and R.B. Marcus, *Oxidation of curved silicon surfaces*, J. Electrochem. Soc. 134 (1987), pp. 481–490.

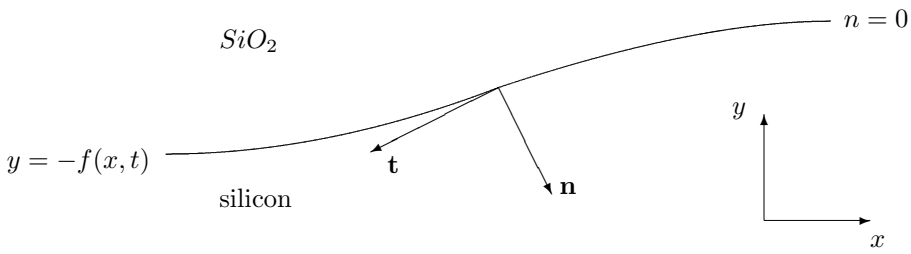


Figure 7: Notation for the Si/SiO$_2$ interface.

# A Stress on the Si/SiO$_2$ boundary in terms of the stream function.

The moving boundary $y = -f(x,t)$ (or $n = 0$) is denoted by the plane curve $\mathbf{r} = \mathbf{r}(s,t) \equiv (x(s,t), y(s,t))$ where $y(s,t) = -f(x(s,t),t)$ and $s$ is arc length. We let $\mathbf{t}$ and $\mathbf{n}$ be the tangential and normal vectors respectively, as shown in Figure 7. If $\theta$ is the angle that $\mathbf{t}$ makes with the horizontal then

$$\mathbf{t} = (-\cos\theta, -\sin\theta), \qquad \mathbf{n} = (\sin\theta, -\cos\theta),$$

and on $n = 0$

$$\frac{\partial x}{\partial s} = -\cos\theta, \quad \frac{\partial y}{\partial s} = -\sin\theta, \quad \frac{\partial x}{\partial n} = \sin\theta, \quad \frac{\partial y}{\partial n} = -\cos\theta,$$

$$\frac{\partial^2 x}{\partial s^2} = \sin\theta\frac{\partial\theta}{\partial s}, \quad \frac{\partial^2 y}{\partial s^2} = -\cos\theta\frac{\partial\theta}{\partial s}, \quad \frac{\partial^2 x}{\partial s\partial n} = \cos\theta\frac{\partial\theta}{\partial s}, \quad \frac{\partial^2 y}{\partial s\partial n} = \sin\theta\frac{\partial\theta}{\partial s}.$$

The chain rule gives

$$\frac{\partial\psi}{\partial s} = -\cos\theta\frac{\partial\psi}{\partial x} - \sin\theta\frac{\partial\psi}{\partial y}, \qquad \frac{\partial\psi}{\partial n} = \sin\theta\frac{\partial\psi}{\partial x} - \cos\theta\frac{\partial\psi}{\partial y},$$

$$\frac{\partial^2\psi}{\partial s\partial n} = \cos\theta\frac{\partial\theta}{\partial s}\frac{\partial\psi}{\partial x} + \sin\theta\frac{\partial\theta}{\partial s}\frac{\partial\psi}{\partial y} - \sin\theta\cos\theta\frac{\partial^2\psi}{\partial x^2} + (\cos^2\theta - \sin^2\theta)\frac{\partial^2\psi}{\partial x\partial y} + \sin\theta\cos\theta\frac{\partial^2\psi}{\partial y^2}.$$

We have

$$\sigma_{nn} = \sigma_{ij}n_i n_j = -p + 2\mu_s\left((\sin^2\theta - \cos^2\theta)\frac{\partial^2\psi}{\partial x\partial y} + \sin\theta\cos\theta\left(\frac{\partial^2\psi}{\partial x^2} - \frac{\partial^2\psi}{\partial y^2}\right)\right),$$

so that

$$\sigma_{nn} = -p - 2\mu_s\left(\frac{\partial^2\psi}{\partial s\partial n} + \frac{\partial\theta}{\partial s}\frac{\partial\psi}{\partial s}\right).$$

Now, the first condition of no slip on $y = -f$ for the flow problem (1.5) gives $\partial\psi/\partial n = 0$, and using the condition in (1.5) for $\partial\psi/\partial s$ together with the usual expression for the curvature of the interface

$$\frac{\partial\theta}{\partial s} = -\frac{\partial^2 f}{\partial x^2}\left(1 + \left(\frac{\partial f}{\partial x}\right)^2\right)^{-3/2},$$

then gives (1.9) as the normal stress on the $Si/SiO_2$ boundary.

# B Nitride rigidity limits

Here we consider the limits of small and large nitride rigidity coefficient, corresponding to a thin (flexible) and a thick (stiff) nitride mask, respectively. Estimates of the nitride rigidity in [11], suggest that $10^{-4} \leq R \leq 10^4$, which motivates the two limits we now take.

(i) Small nitride rigidity. In the limit $R \to 0$ we have $p_0 = O(R)$ and thus for $(\alpha_k, \alpha_d) = O(1)$, the stresses in the oxide are not sufficiently large to affect the reaction coefficient at leading order (in $R$) and the results for the stress independent case apply. Consequently, we rescale as follows $\hat{\alpha}_k = R\alpha_k, \hat{\alpha}_d = R\alpha_d$, so that in $X = O(1)$, we pose the expansions

$$f_0 = \hat{f}_0 + O(R), \qquad \eta_0 = \hat{\eta}_0 + O(R),$$

to obtain

$$\hat{\eta}_0 = (\gamma - 1)\hat{f}_0 + 1,$$

and

$$\frac{\partial \hat{f}_0}{\partial \tau} = \frac{\partial}{\partial X}\left((\gamma \hat{f}_0 + 1) D_{s0}(\hat{p}_0) \frac{\partial}{\partial X}\left(\frac{1}{\kappa_{s0}(\hat{p}_0)} \frac{\partial \hat{f}_0}{\partial \tau}\right)\right), \tag{B.25}$$

together with

$$\text{at } X = 0 \qquad \hat{f}_0 = \frac{\kappa_0}{\gamma}\tau, \quad \frac{\partial^2 \hat{f}_0}{\partial X^2} = \frac{\partial^3 \hat{f}_0}{\partial X^3} = \frac{\partial^4 \hat{f}_0}{\partial X^4} = 0,$$

and

$$\text{as } X \to +\infty \qquad \hat{f}_0 \to 0, \qquad \text{at } \tau = 0 \qquad \hat{f}_0 = 0.$$

Here,

$$\hat{p}_0 = (\gamma - 1)\frac{\partial^4 \hat{f}_0}{\partial X^4} \tag{B.26}$$

and now

$$\kappa_{s0} = \begin{cases} \kappa_0 e^{-\hat{\alpha}_k \hat{p}_0}, & \text{if } \hat{p}_0 > 0, \\ \kappa_0, & \text{if } \hat{p}_0 \le 0, \end{cases} \qquad D_{s0} = \begin{cases} e^{-\hat{\alpha}_d \hat{p}_0}, & \text{if } \hat{p}_0 > 0, \\ 1, & \text{if } \hat{p}_0 \le 0. \end{cases}$$

From (B.25), (B.26), the problem can be written as a novel single high order evolution equation for $\hat{f}_0$.
(ii) Large nitride rigidity. In the limit $R \to \infty$, the nitride acts at leading order as if it were rigid, i.e.

$$\eta_0 = 1 + o(1).$$

Writing

$$\frac{\partial^2 \eta_0}{\partial X^2} = \frac{1}{R}\zeta \quad \text{and} \quad f_0 = \bar{f}_0 + O(1/R), \tag{B.27}$$

(2.3) then gives at leading order,

$$\frac{\partial \bar{f}_0}{\partial \tau} = \frac{\partial}{\partial X}\left((1 + \bar{f}_0) D_{s0} \frac{\partial}{\partial X}\left(\frac{1}{\kappa_{s0}} \frac{\partial \bar{f}_0}{\partial \tau}\right)\right), \tag{B.28}$$

together with (2.5)–(2.7), and (2.9)–(2.12) become

$$-(\gamma - 1)\frac{\partial \bar{f}_0}{\partial \tau} = \frac{1}{12}\frac{\partial}{\partial X}\left((1 + \bar{f}_0)^3 \frac{1}{\mu_{s0}} \frac{\partial^3 \zeta}{\partial X^3}\right), \tag{B.29}$$

$$\text{at } X = 0 \quad \zeta = \frac{\partial \zeta}{\partial X} = \frac{\partial^2 \zeta}{\partial X^2} = 0, \qquad \text{as } X \to +\infty \quad \frac{\partial^3 \zeta}{\partial X^3} \to 0. \tag{B.30}$$

This system is better rewritten in terms of the pressure $p_0 = \zeta_{XX}$, as follows

$$\frac{\partial \bar{f}_0}{\partial \tau} = \frac{\partial}{\partial X}\left((1 + \bar{f}_0)\frac{\partial}{\partial X}\left(\frac{1}{\kappa_{s0}(p_0)} \frac{\partial \bar{f}_0}{\partial \tau}\right)\right), \quad \frac{\partial p_0}{\partial X} = -\frac{12(\gamma - 1)}{(1 + \bar{f}_0)^2} \frac{D_{s0}(p_0)}{\mu_{s0}(p_0)} \frac{\partial}{\partial X}\left(\frac{1}{\kappa_{s0}(p_0)} \frac{\partial \bar{f}_0}{\partial \tau}\right), \tag{B.31}$$

$$\text{at } X = 0 \quad \bar{f}_0 = \frac{\kappa_0}{\gamma}\tau, \; p_0 = 0, \qquad \text{as } X \to +\infty \quad \bar{f}_0 \to 0, \qquad \text{at } \tau = 0 \quad \bar{f}_0 = 0, \tag{B.32}$$

with $\int_0^\infty p_0 \, dX = 0$, corresponding to the requirement that the net upward force on the nitride be zero. To obtain (B.31), (B.28) and (B.29) have been used, together with the condition in (B.30).

The solution in this region will not satisfy $p_0 = \zeta_{XX} \to 0$ as $X \to \infty$. To fully determine it, an additional region is required with scaling $X = R^{1/6}\chi$. In $\chi = O(1)$, $\bar{f}_0$ is exponentially small, and thus we pose

$$\eta_0 \sim 1 + R^{-1/3}\eta^*,$$

with

$$\frac{\partial \eta^*}{\partial \tau} = \frac{1}{12}\frac{\partial^6 \eta^*}{\partial \chi^6},$$

$$\text{at } \chi = 0 \qquad \frac{\partial^2 \eta^*}{\partial \chi^2} = \frac{\partial^3 \eta^*}{\partial \chi^3} = 0, \quad \frac{\partial^4 \eta^*}{\partial \chi^4} = \lim_{X \to \infty} \frac{\partial \zeta}{\partial X^2},$$

$$\text{as } \chi \to +\infty \quad \eta^* \to 0, \qquad \text{at } \tau = 0 \quad \eta^* = 0.$$

The leading order pressure in this region is $p_0 = \eta^*_{XXXX}$, which is $O(1)$, implying that the largest stresses occur in both this and the $X = O(1)$ regions.

# C Cylindrical oxidation for large initial radii

Here we examine the limit of large initial radii in the regime of cylindrical oxidation considered in section 3.1. The spherical case is similar, with analogous results also holding for the cavity case of section 3.2. We introduce a small parameter $\epsilon > 0$ through the scaling of the initial $Si/SiO_2$ interface

$$d_0 = \frac{\bar{d}_0}{\epsilon},$$

where $\bar{d}_0 = O(1)$, and thus $b_0 = \frac{\bar{d}_0}{\epsilon} + 1$. Posing

$$d = \frac{\bar{d}_0}{\epsilon} + d_1 + O(\epsilon), \qquad b = \frac{\bar{d}_0}{\epsilon} + 1 + b_1 + O(\epsilon),$$

as $\epsilon \to 0$, then (3.7) gives

$$b_1 = -(\gamma - 1)d_1$$

and (3.5) can yields

$$\dot{d}_1 \left(1 + D_s \left(\frac{1}{k_s} + \frac{1}{H}\right) - \gamma d_1\right) = -\frac{1}{\gamma}. \tag{C.1}$$

Now the normal stress (3.11) and pressure are

$$\sigma_{nn} \sim -\frac{4}{\bar{d}_0^2}\epsilon \dot{b}_1(1 - \gamma d_1), \qquad p \sim -2\epsilon \dot{b}_1,$$

which are both small. Thus, if the stress dependent parameters $\alpha_k, \alpha_d$ are $O(1)$, then the reaction and diffusion coefficients are their stress free values. Consequently $k_s = k_0, D_s = 1$ and (C.1) may be integrated to give

$$\frac{\gamma}{2}d_1^2 - \left(1 + \frac{1}{k_0} + \frac{1}{H}\right) d_1 = \frac{t}{\gamma}, \tag{C.2}$$

using $d_1(0) = 0$, which is the one-dimensional Deal-Grove solution. It may also be stated in terms of the leading order oxide thickness $r_0 = 1 + b_1 - d_1 = 1 - \gamma d_1$, giving a dimensionless expression analogous to that in [9, 35]. The stress dependent coefficients thus have little effect for large radii, unless the parameters $\alpha_k, \alpha_d, \alpha_\nu$ are large and $O(1/\epsilon)$. This is consistent with the experimental results of [16], where stress inhibited growth is more significant for small radii.